Stanford Exploration Project, Report 94, November 11, 1997, pages 1–16

Characterization of a hydrate reservoir

Christine Ecker[1]

keywords: *AVO, reservoir characterization, hydrates*

ABSTRACT

I use marine seismic data from the Blake Outer Ridge region to characterize the lateral distribution of a methane hydrate reservoir. Detailed amplitude versus offset (AVO) analysis of the data, combined with velocity analysis and seismic impedance inversion is used to explore the extend and characteristic of the bottom simulating reflector (BSR) associated with the base of the hydrate stability field. The results suggest a strong correlation between strong BSR reflections and the presence of a low velocity zone. This is indicative of the presence of free gas beneath the hydrate. Weaker BSR amplitudes occur in areas of decreased velocity contrasts and "fractured" appearance of the BSR. The P-impedance inversion results in strong contrasts both at the seafloor and the BSR due to the significant velocity contrasts there. The S-wave impedance contrast, on the other hand, shows a stronger contrast in the vicinity of the BSR than at the seafloor. The BSR contrast has a rather irregular appearance and seems to be dominated by events cutting in from underneath. These events are significantly weaker in the P-impedance contrast and are partly not even visible. AVO analysis of the amplitudes at three different locations along the BSR resulted in decreasing P-wave velocities across the BSR and S-wave velocities that are either increasing, decreasing or unchanged. Possible reasons for these local variations of the shear wave velocity might be either patchy hydrate saturation or patchy gas saturation beneath the hydrate. Furthermore, the hydrate might be fractured, thus causing the properties of the hydrate to change locally.

INTRODUCTION

The interest in methane hydrates as a potential future energy resource has been constantly increasing during recent years. Assessments show that worldwide there might be twice as much hydrocarbon available from hydrate resources than from all known recoverable and non-recoverable coal, oil and gas deposits (Kvenvolden, 1993). Recent drilling at the Blake Outer Ridge offshore Florida and Georgia has shown that there might be as much as 4.7 x 10^{16} g CH_4, or 35 GT of carbon available there. This

[1]**email:** christin@sep.stanford.edu

quantity could meet the 1996 United States natural gas consumption needs for the next 105 years (Dickens et al., 1997).

In order to evaluate the future impact of methane hydrates realistically, it is essential that we understand its elastic and mechanical properties. Information available from surface seismic and drilling has to be linked with rock physics to estimate the amount of hydrate present, its distribution in the pore space, permeability and potential recoverability (Lee et al., 1992; Dvorkin and Nur, 1993; Ecker and Lumley, 1994; Ecker et al., 1996; Andreassen et al., 1995). Most studies were restricted to using only the P-wave velocity information to infer those properties, assuming a known in-situ hydrate Poisson's ratio based on laboratory studies. However, when trying to assess hydrate structures, S-wave velocity behavior might be an important piece of information that can influence the estimated hydrate properties significantly (Ecker et al., 1996). Therefore, it is essential to perform an integrated characterization using as much information as possible.

In this paper I present the characterization of a hydrate reserve at the Blake Outer Ridge offshore Florida and Georgia using both compressional and shear information contained in the data. Part of the data have been described in previous reports (Ecker and Lumley, 1994b; Ecker, 1995). Data preprocessing includes spherical divergence correction, source wavelet deconvolution and amplitude calibration. The seafloor multiple was used to normalize the zero-offset amplitudes, thus resulting in an zero offset, reflection strength map of the section. A detailed NMO stacking velocity analysis was performed to infer the P-wave velocity structure. Subsequently, I applied AVO analysis on the data, followed by a true amplitude migration/inversion. The results show strong variations in the zero-offset reflection coefficient of the BSR. The strongest BSR amplitudes seem to coincide with the presence of a low velocity zone. Weak BSR reflections occur over an area of diminished velocity contrasts and discontinuous hydrate appearance. The impedance inversion results suggest very strong P-impedance contrasts at the BSR and the seafloor, dominating the entire seismic section. The S-impedance contrast shows a strong contrast at the BSR compared to the seafloor. The data show a significant spread of BSR AVO responses laterally. This might be partly due to interference with underlaying structure, patchy hydrate or gas saturation or fracturing that affects the hydrate locally.

PREPROCESSING

The data were processed to preserve true amplitude information. In the first step, they were corrected for time-varying spherical divergence correction. Then I performed a single-trace source wavelet deconvolution in order to regularize the source wavelet with offset. The deconvolved data was then bandpass filtered to the original data bandwidth to remove spurious deconvolutional high-frequency noise. Using NMO stacking analysis, I obtained a 2-D velocity field for the data by picking velocities every 25th supergather, which consisted of 10 averaged adjacent gathers. A smoothed version was then used as input into a true amplitude prestack migration (Lumley and

Beydoun, 1993). A residual moveout correction was subsequently applied to the migrated, NMO corrected gathers to correct events that could not be completely flattened using the stacking velocities. Since it is essential that the reflector moveout is very flat for AVO analysis, an additional static shift was applied to correct for some small, non-hyperbolic offset-dependent residual moveout in the CMP gathers after migration.

In order to recover the true amplitude information in the data, I calibrated the data amplitudes using the seafloor as a reference reflection. First I normalized each CMP gather by the near-offset seafloor amplitude. I then calibrated the amplitudes assuming a functional form of the seafloor AVO response. Results from drilling in the area suggest that the P-wave velocity increases from about 1.45 to 1.5 km/s and the density from 1.0 g/ccm to approximately 1.3-1.4 g/ccm (Matsumoto et al., 1996; Ecker, 1997). The implementation of a dipole shear wave tool during the deeper drilling in the sediment implies very low S-wave velocities in the area caused by highly unconsolidated, shaly sediments. Based on this information and following Hamilton (Hamilton, 1976), I assumed an S-wave velocity of about 0.25 km/s for the shallow sediments. Using these elastic properties, I determined an angle-dependent correction function for the data, which forced the seafloor AVO to decrease slightly (nearly constant) with increasing offset. A migrated and amplitude corrected CMP gather can be seen in Figure 1.

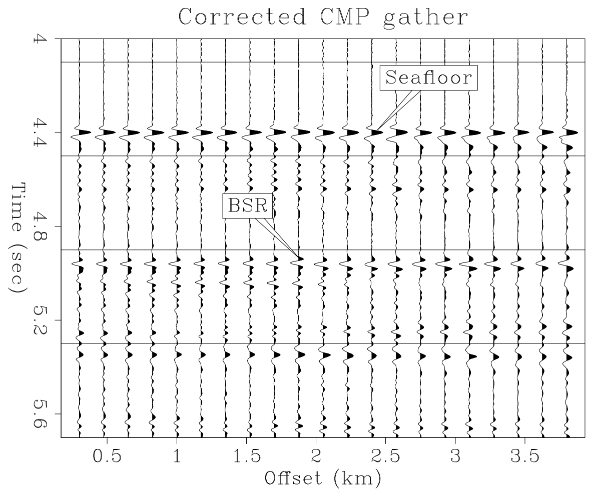

Figure 1: Final CMP gather after migration and all calibrations were applied to the data. The three main events are the seafloor, the BSR and the flat reflector underneath. christin2-gather-ann [CR]

DATA

The data consist of 1105 CMP gathers with a midpoint spacing of 50 m. The near offset is at 0.3 km and the far offset is at 3.9 km. The offset spacing is 50 m. A stacked section of the data after migration can be seen in the upper panel of Figure 2. It shows a strong seafloor reflection of more than 4s two-way travel time, suggesting a water depth of more than 3 km. It is partly underlain by a BSR reflection of opposite polarity. This is the reflection of the base of the hydrate stability field. Above the

BSR, methane hydrate is present in the pore space of the sediment, while underneath the BSR the sediment is saturated with free gas. The presence of free gas has been suggested in a study by Ecker and Lumley (Ecker and Lumley, 1994) and proofed by the recent ODP drilling in the area. The BSR appears to stop at a distance between 25 and 30 km. There it merges together with a reflection from underneath what probably coincides with the bottom of the free gas zone (Ecker and Lumley, 1994). Shortly before both reflectors come together, the BSR splits with one part overlaying the other, suggesting a discontinuous reflection character.

A high frequency stack of the data which was obtained by high-pass filtering the data to frequencies above 40 Hz can be seen in the lower panel of Figure 2. It displays a significant amount of "thin layering" effects underneath the BSR, in particular where the normal stacked section showed a separation of the BSR in an upper and lower part. The BSR appears to be fractured and shows partly strong interferences with the small thin structures underneath. This indicates that the reduction of frequency content by either temporal or spatial (stacking) filtering produces a more apparent lateral continuity of the BSR due to the Fresnel zone. The same effect was observed by Lee et al. (1994) in this area. The thin layering visible underneath and cutting against the BSR is suggestive of rapid lateral variations immediately beneath the BSR. There might be 3-D features, such as gas pockets, that contribute scattering or side-swipe energy which cannot be sufficiently processed using 2-D methods.

Velocity and Reflection Amplitude

Interval velocities along the section were obtained from the RMS stacking velocities using Dix's equation. The resulting 2-D velocity field, overlain by the stacked section, can be seen in Figure 3. It shows an increase in the velocity above the BSR to about 1.9 km/s and a decrease to approximately 1.55-1.6 km/s underneath. The presence of hydrate in sediments is often associated with an increase of velocity. The low-velocity zone beneath it is indicative of the sediments being gas saturated. The accumulation of free gas beneath the BSR can be explained by the hydrate acting as impermeable seal (Ecker et al., 1996) and thus trapping the gas underneath. The velocity contrast becomes less and less pronounced closer to the termination point of the BSR at approximately 25 km. Both the absence of free gas underneath the hydrate and the possible reduction of the amount of hydrate present can be related to this decrease in velocity contrast.

In order to get an idea of the magnitude of the amplitude variation in the area, and in order to be able to scale the amplitudes in the later AVO analysis, I used the first multiple of the seafloor to calculate the reflectance of the reflections. In a layered medium, this reflectance is similar to the true reflection coefficient (Warner, 1990):

$$R_w = \frac{A_m}{A_w} \text{ and } R_i = \frac{A_i}{A_w} R_w$$

where R_w is the reflection coefficient of the seafloor, A_w is the amplitude of the seafloor reflection and A_m that of its first multiple. The reflection coefficient of the

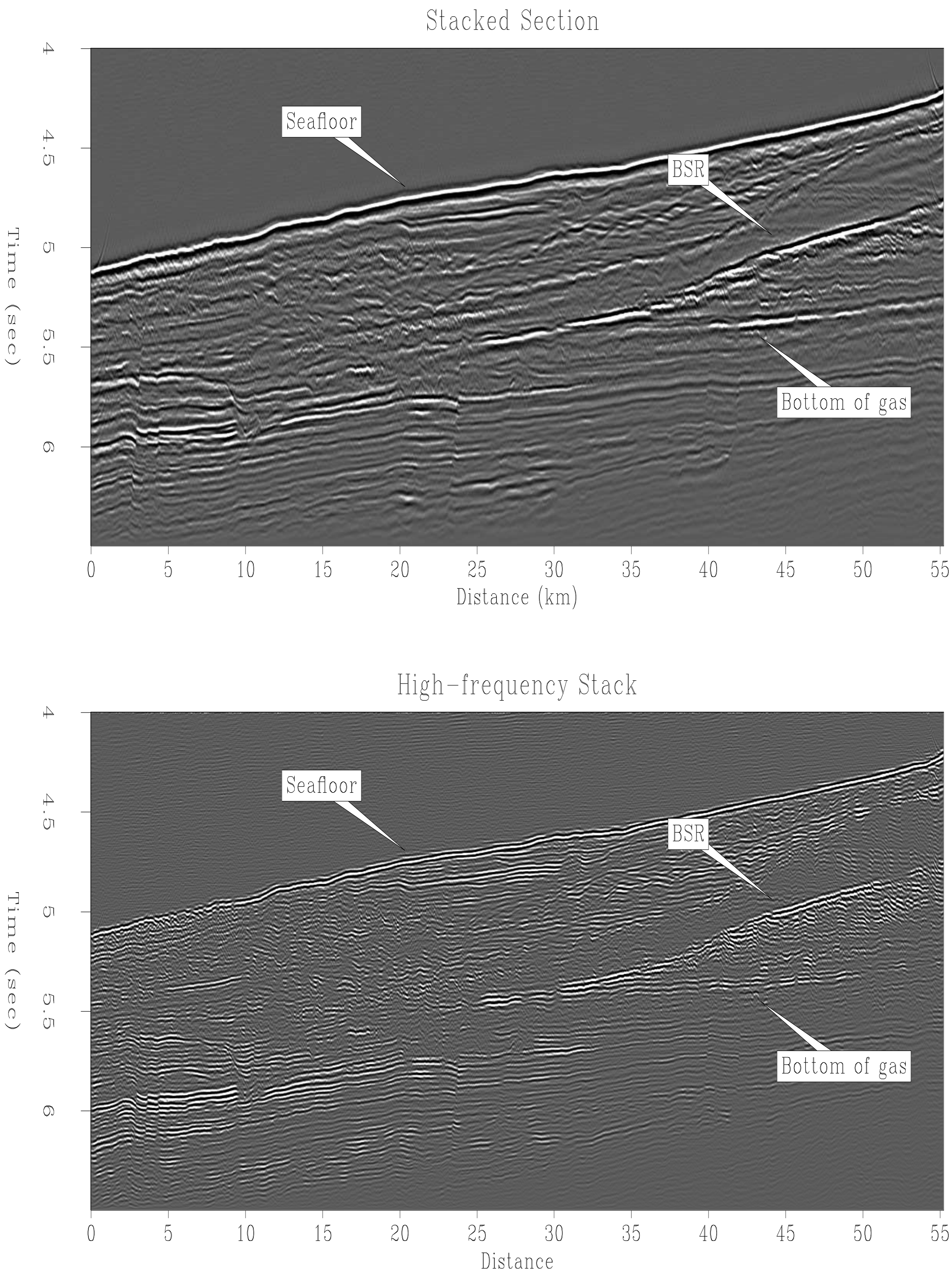

Figure 2: The upper panel shows a migrated stacked section of the data. High-pass filtering to frequencies above 40 Hz resulted in the high-frequency stack displayed in the lower panel. christin2-data [CR]

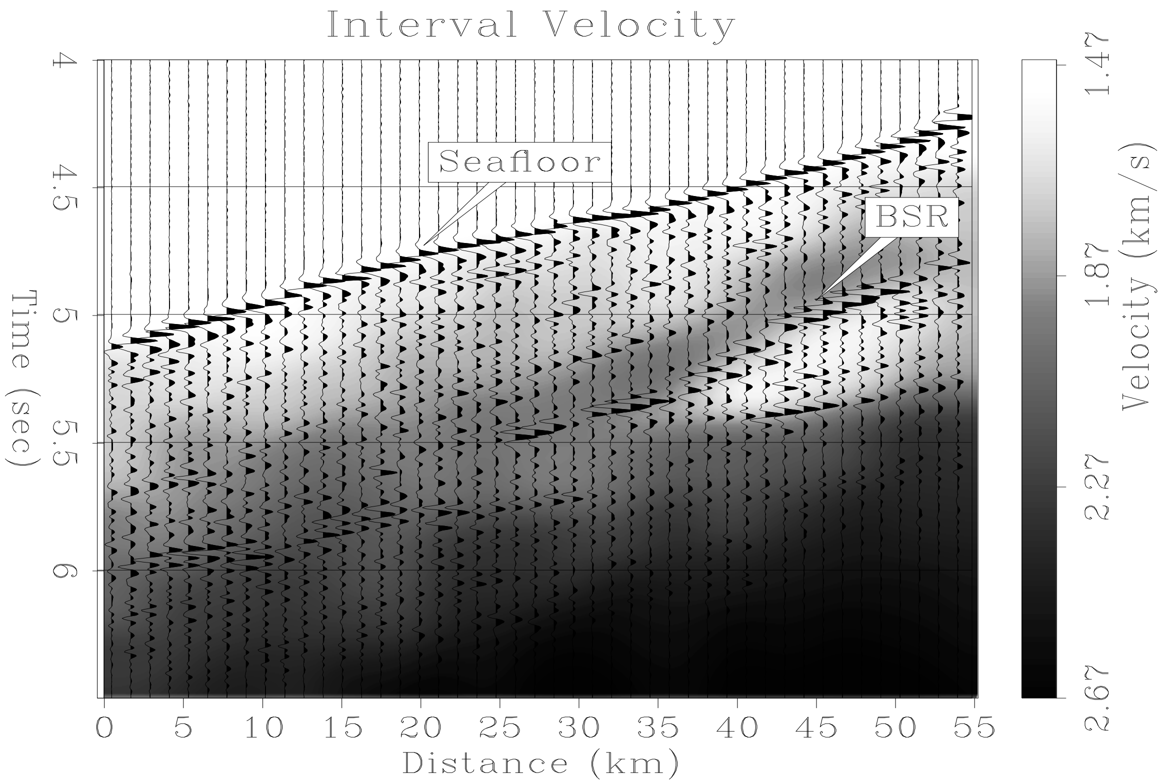

Figure 3: Interval velocity of the data. christin2-vint-ann [CR]

ith layer is given by R_i and A_i is the amplitude of the ith reflection. The resulting 2-D reflection amplitude map can be seen in Figure 4. It is obvious that the strong BSR reflection coincides with the free gas trapped beneath the BSR. Picking the maximum BSR amplitudes (Figure 5) shows that the amplitude is nearly twice as strong between 45 and 50 km than elsewhere. The decrease of amplitudes in the region of BSR discontinuity (between 35 and 45 km) might be related some change of the local hydrate properties in the area. At the flank of the BSR the decrease is caused by the decreasing velocity contrast. The absence of free gas in itself will already cause the impedance contrast to be significantly weaker in this area. Furthermore, the amount of hydrate in the sediment might be decreasing, thus not inducing enough velocity increase in the hydrate. There might be less hydrate in the sediment pore space, causing a less pronounced velocity contrast. The ODP drilling in the area recovered hydrate even from regions without apparent BSR in surface seismic (Matsumoto et al., 1996). This appears to support the fact that the amount of hydrate occupying the pore space might be decreasing.

IMPEDANCE INVERSION

To evaluate the behavior of P- and S-impedance contrast across the different BSR sections and the gas zone, I performed a least-squares elastic parameter inversion

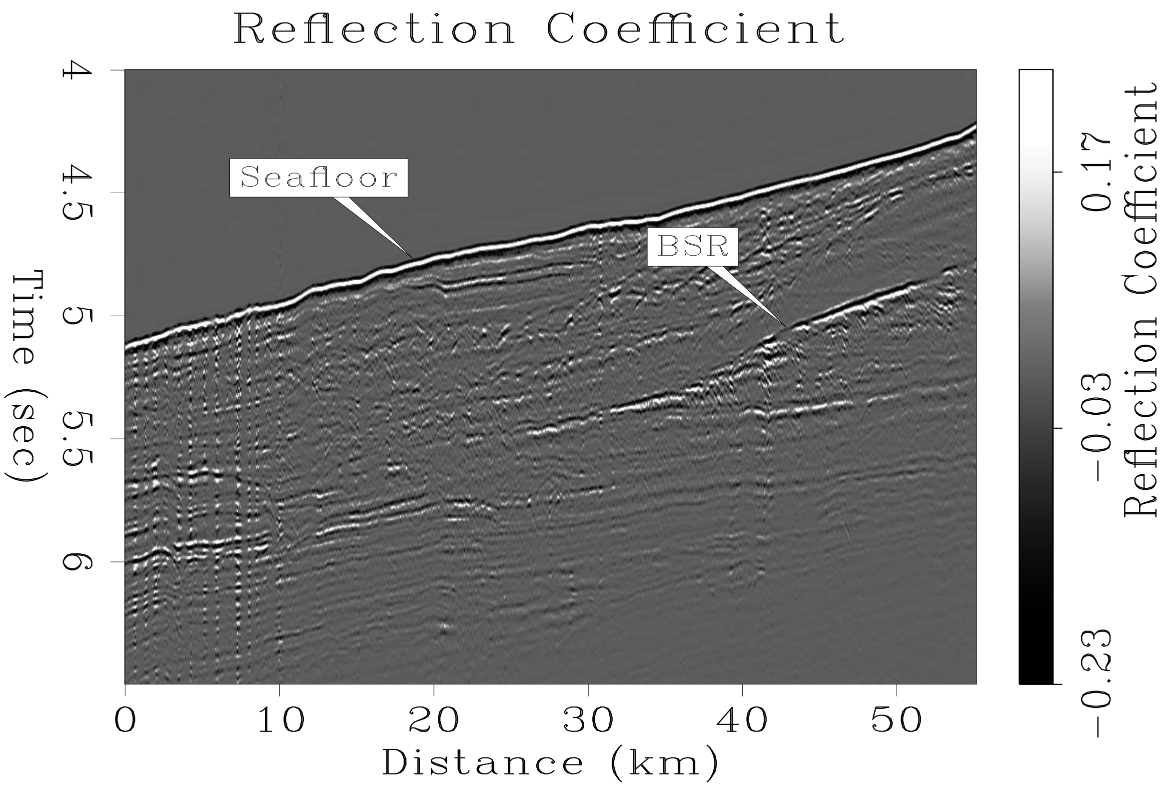

Figure 4: Zero offset reflection amplitudes obtained using the first multiple of the seafloor reflection. christin2-reflection-ann [ER]

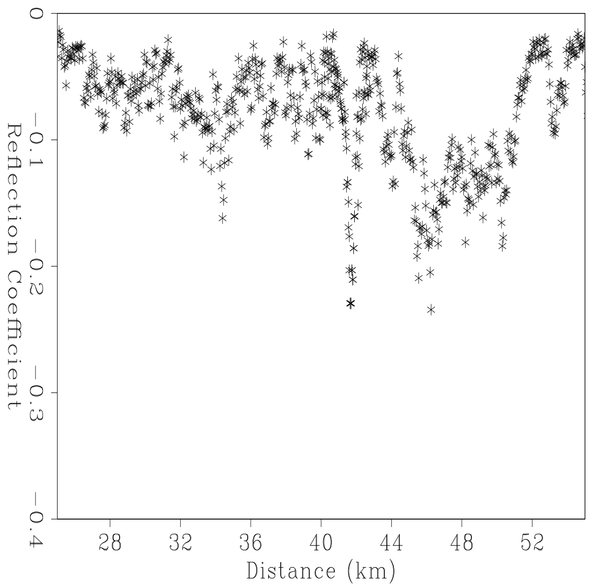

Figure 5: Amplitude picks along the BSR. christin2-bsr-picks [ER]

(Lumley, 1993). This technique fits the prestack migrated AVO gathers at each pseudo-depth and surface position to the theoretical P- and S-impedance curves based on linearized Zoeppritz equations (Aki and Richards, 1980):

$$R(\theta) \;=\; \frac{1}{2\cos^2(\theta)}\, I_p \;-\; 4\,\gamma^2\,\sin^2(\theta)\, I_s + (2\gamma^2\,\sin^2(\theta) \;-\; \tfrac{1}{2}\,\tan^2(\theta))\, D$$

where $R(\theta)$ is the reflectivity, θ is the angle of incidence, I_p and I_s are the P-impedance and S-impedance contrasts, respectively. The density contrast is given by D and γ is the background $\frac{v_s}{v_p}$ ratio. Since the term depending on the density contrast will only contribute for angles above 40 degrees, it is not used here. The maximum angle of the data is not larger than 33 degrees. Based on the drilling information in the area, I choose a γ^2 of about 0.1 since the sediments display overall low S-wave velocity character (Ecker, 1997). The inversion results are shown in Figures 6 and 7.

The P-impedance section clearly shows both a strong seafloor and a strong BSR contrast of opposite polarity but comparable magnitude. The negative contrast at the BSR is caused by the decrease of the velocity at the transition from hydrated sediment to gas-saturated sediment. The contrast at the BSR is strongest between 45 and 50 km, as was expected from the velocity analysis and the amplitude behavior. Significantly less contrast is displayed in the area of BSR discontinuity (between 35 and 40 km).

The S-impedance contrast shows that the BSR has a significantly higher contrasts than the seafloor. As opposed to the very continuous P-impedance contrast along parts of the BSR, the S-impedance contrast displays a very fractured character. Strong contrasts are obtained from the rapid structure underneath the BSR which is interfering with the BSR contrast itself. In areas of small interference, the BSR contrast is of the same polarity as the seafloor, implying a positive impedance contrast. One reason for the P-impedance map not to show this fracturing effect might either be that those structures do not have an effect in P-impedance, or it is so small compared to the one of the BSR that it is not visible in the impedance map. The effects on P-wave velocity and density could cancel each other out. Since it is mainly visible in the S-impedance contrast section, this means that there is a pronounced contrast in shear moduli or density.

The differences between P-impedance and S-impedance behavior are more pronounced on a simple P*S impedance map as shown in Figure 8. Impedances of the same sign are plotted as blue, while impedance contrasts of opposite behavior are plotted as red. Between 40 and 50 km, the BSR is characterized by laterally varying contrasts. If there is no strong interference with the underlaying structure, P- and S-impedance appear to have the opposite sign, thus indicating a negative P-impedance contrast but a positive S-impedance contrast. The structure underneath the BSR shows P- and S-impedance contrasts of the same sign, however. The flank of the BSR between 35 and 25 km seems to show that most of the P- and S-impedance contrasts behave equally (either increasing or decreasing).

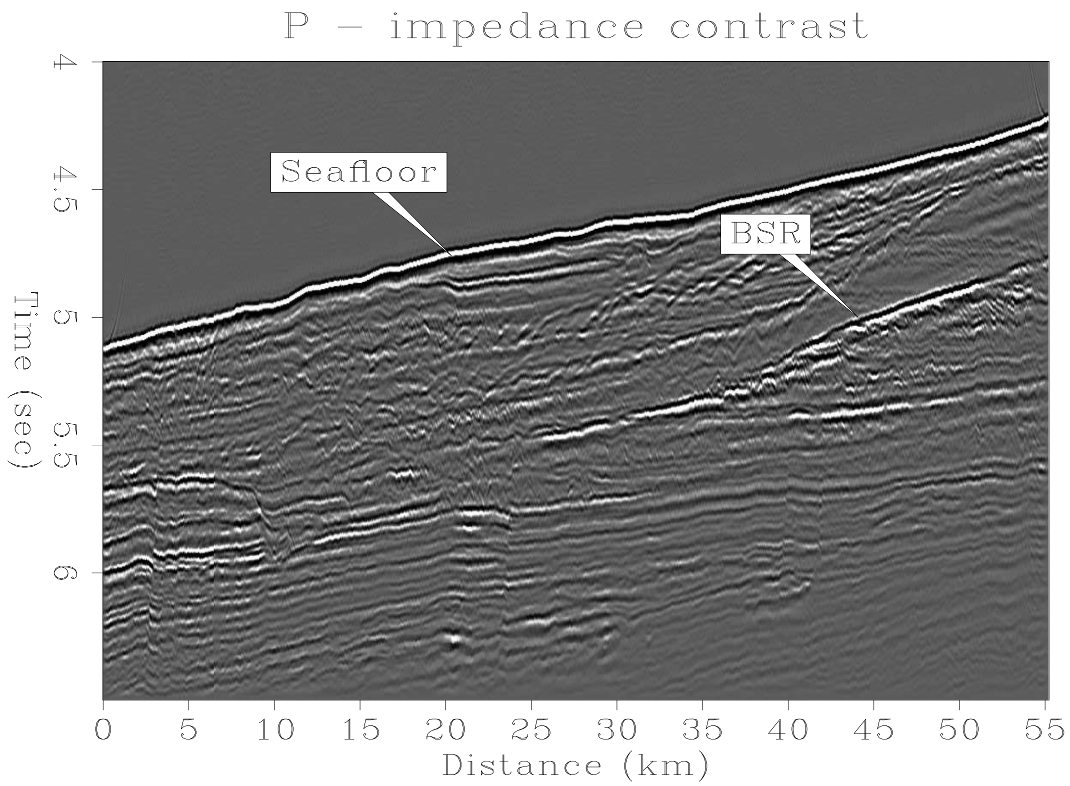

Figure 6: P-impedance contrast section. christin2-pmp-ann [CR]

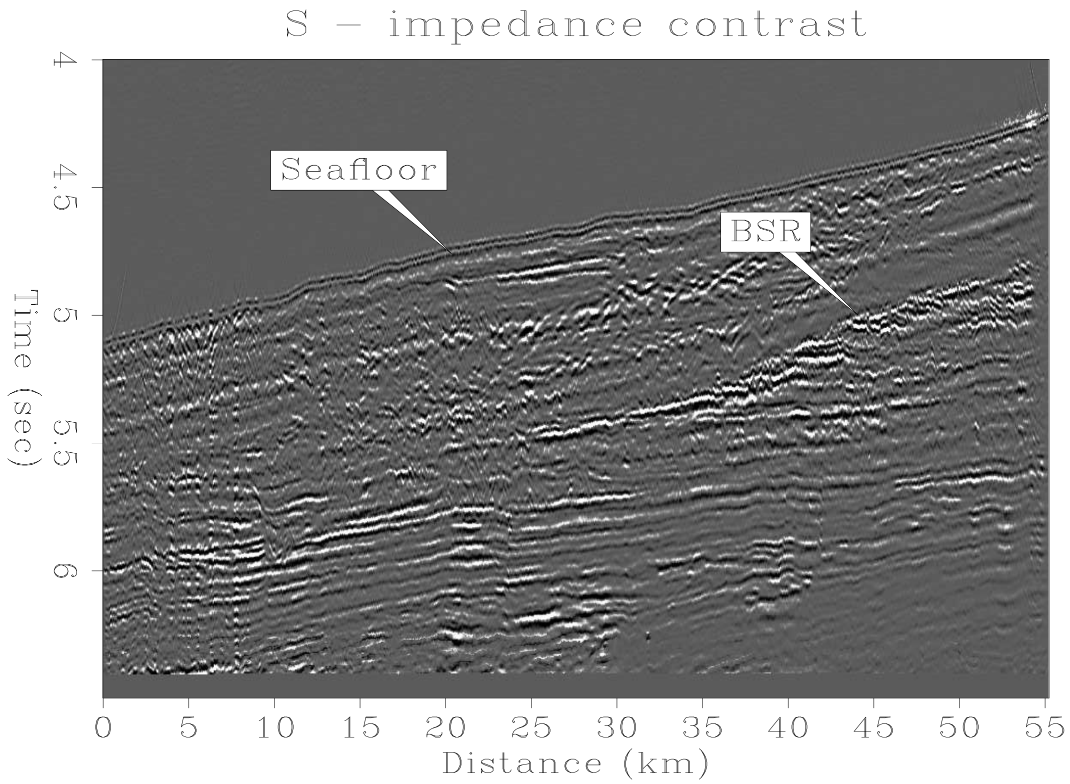

Figure 7: S-impedance contrast section. christin2-simp-ann [CR]

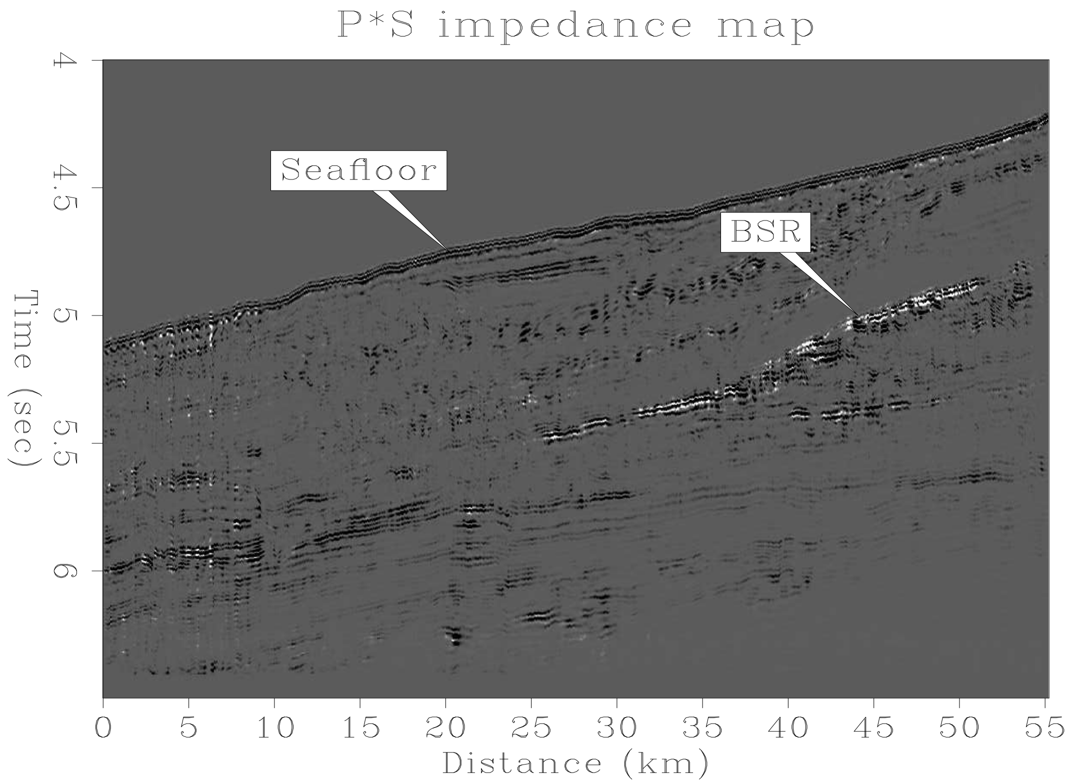

Figure 8: P*S impedance contrast section. christin2-PSmap-ann [CR]

AVO MODELING

The 2-D impedance inversion has shown that the hydrate appears to significantly change its lateral characteristic. This structure might be either related to the hydrate itself and its changing properties and occurrence in the pore space, or some real structure beneath the BSR. In order to evaluate the obtained impedance contrasts more in terms of velocity contrast, I explored which velocity/impedance model could reproduce the AVO data locally at three different BSR structures. To minimize the variation and noise of the data, I assumed that in the area I chose the local lithology properties do not vary within at least 150 m. Thus I used at least three adjacent CMP gathers to average my amplitude response. Several velocity models were constructed that were constrained to preserve the average interval velocity of the area. The density contrast across the BSR is assumed to be known and held constant in the modeling. Since the density of pure hydrate is significantly larger than that of gas, I assumed a slight decrease in the density at the BSR. This is supported by the well data in the area (Ecker, 1997). Synthetic AVO responses were then estimated for the individual models using Zoeppritz equations and compared with the seismic data. I have shown in the other paper included in this report (Ecker, 1997) that local AVO analysis is rather robust for the estimation of the acoustic properties, but can include a significant error for the S-wave properties depending on the variance of the data.

Thus, several models might fit the data within a reasonable error bound and I will give a possible range as an error estimate.

In the first model, I picked the amplitude at a place of opposite P- and S-impedance contrasts at 50 km distance. The picked amplitudes as seen in the left panel of Figure 9, are increasingly negative with increasing angle. The modeling shows that his is consistent with a decrease in P-wave velocity of approximately 400 m/s across the BSR and a simultaneous increase in S-wave velocity of about 150 m/s. The best fit obtained from Zoeppritz modeling is overlain with the data. In order to give an idea about the goodness of fit, I plot in the right panel of Figure 9 how the curves would look like for changes in the S-wave velocity contrast of ± 100 m/s. A similar results was obtained in a previous study of part of the data (Ecker and Lumley, 1994) and explained by the sediment containing hydrate to be uncemented and thus mechanically weak (Ecker et al., 1996).

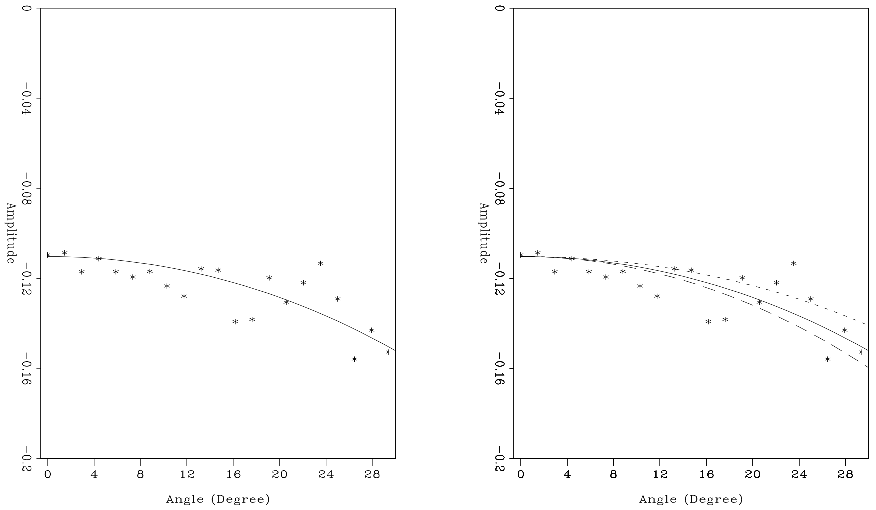

Figure 9: Picked amplitudes along the BSR. The best fit is modeled using Zoeppritz equations and overlain on the picks on the left panel. The right panel shows additional the possible errors bounds of the fit. christin2-increase [ER]

The next AVO picks were obtained at a distance of about 47 km, in an area of event interference. The amplitudes show a trend which is clearly opposed to the previous one. Instead of increasing with increasing offset, the amplitudes decrease. Modeling this behavior results again in a significantly large negative P-impedance contrast, but an S-contrast of the same sign (Figure 10). The best data fit suggest a decrease in S-wave velocity of about 300 m/s. Considering the data variations this would be determined within a ± 50 m/s bound as seen in the right side of Figure 10. This model indicates a completely different hydrate behavior than before. However, it must be carefully evaluated since the amplitude trend might have been distorted from interference, and thus might not represent the actual BSR trend. A possible explanation for this kind of behavior might be that the hydrate is not underlain by gas but by brine saturated sediment in this area. Due to the increase in density, this would lead to a positive S-wave velocity contrast.

In the third modeling evaluation, I picked the amplitudes at a section near the flank of the BSR (35 km). The amplitudes display a trend which is between the two previous responses. The AVO modeling results in a velocity model that again has a negative, but smaller P-wave velocity contrast across the BSR. The best data fit is reached with a zero shear wave contrast, meaning that there is no change in the shear wave velocity and density across the BSR. The error bounds suggest a ± 50 m/s limit on the amplitudes, which can mean that there is either a small positive or a small negative contrast. This might support the hypothesis of only a small amount of hydrate saturation of the sediments in this area.

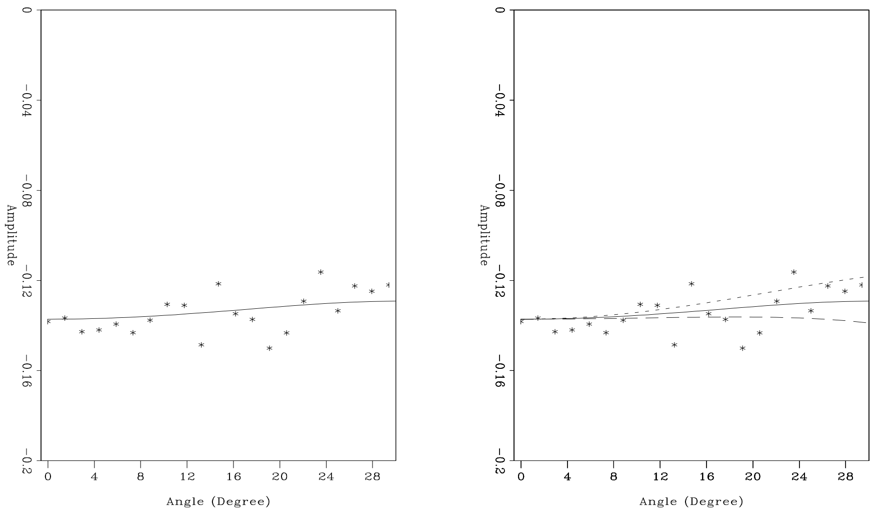

Figure 10: Picked amplitudes along the BSR. The best fit of the data, obtained from Zoeppritz equations, is overlain with the picks. The right side of the picture shows the errors bounds for the fit. christin2-decrease [ER]

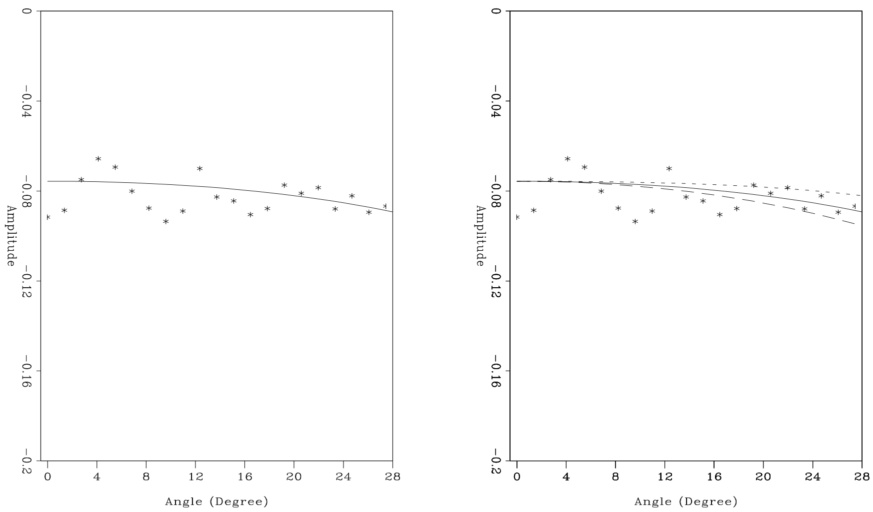

Figure 11: Picked amplitudes along the BSR. The bet data fit is overlain on the left side and shows the appropriate errors limits on the right side. christin2-equal [ER]

The different velocity at the three BSR sections (strong, interfering, flank) are displayed in Figure 12. It is obvious that while the P-wave velocity change stays approximately the same, at least in sign, there is considerable change in the shear wave behavior.

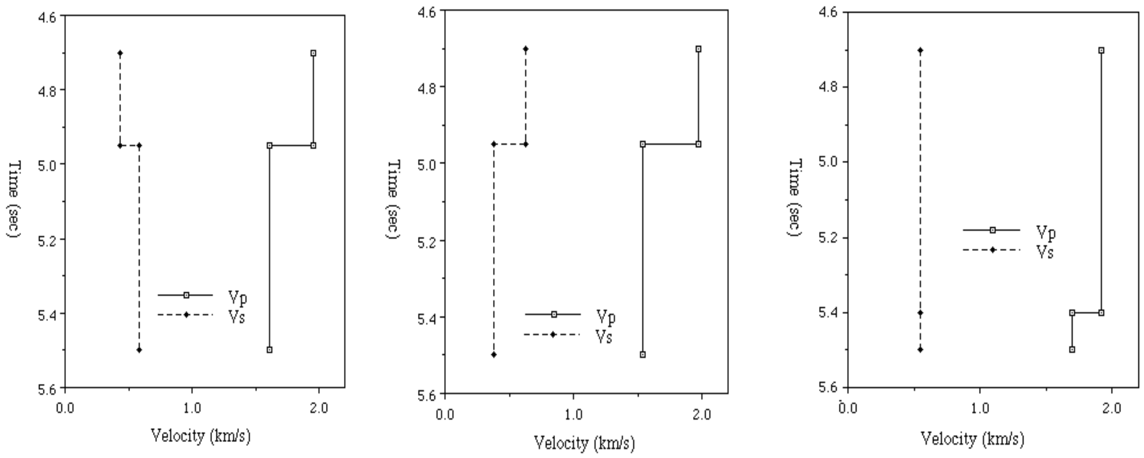

Figure 12: P- and S-wave velocity models obtained from the AVO analysis. christin2-bsr [NR]

CONCLUSIONS

I have used marine seismic data from the Blake Outer Ridge to characterize the lateral variation of a methane hydrate reservoir. The results show that there is a strong correlation between strong BSR amplitudes and the presence of free gas underneath the hydrate. Weaker BSR reflections appear to be associated with both the absence of gas and probable decrease in amount of hydrate present. The P-impedance inversion results in strong contrasts both at the seafloor and the BSR. They are opposite in polarity because of the velocity decrease at the BSR which is partly underlain by free gas. The S-wave impedance contrast, on the other hand, shows a stronger contrast than the seafloor. Furthermore, it displays a significant amount of fracturing of the BSR and considerable contrasts from events underneath the BSR. Forward AVO modeling of CMP amplitudes at three distinct areas of the BSR result in P-wave velocity models that always show a decrease in P-velocity across the BSR, and S-wave velocities that are either increasing, decreasing or equal. At this point, I can only speculate as to what might cause these different responses in velocities and the laterally varying BSR characteristics. One possibility would be the patchy, heterogeneous distribution of hydrate and also the gas underneath. The gas underlying the BSR might occur in bubbles, trapped between small discontinuities, thus changing the elastic moduli. Furthermore, possible fracturing of the hydrate zone itself might cause part of the hydrates close to the fractures to partly destabilize due to the influx of warmer fluid. This could also affect the inferred properties.

REFERENCES

Aki, K., and Richards, P. G., 1980, Quantitative seismology: Theory and methods: W. H. Freeman and Co., New York.

Andreassen, K., Hart, P. E., and Grantz, A., 1995, Seismic studies of a bottom simulating reflector related to gas hydrate beneath a continental margin of the Beaufort Sea: Jour. Geophys. Res., **100**, 12659–12673.

Dickens, G. R., Paull, C. K., Wallace, P., and the ODP Leg 164 Scientific Party, 1997, Direct measurement of in situ methane quantities in a large gas-hydra te reservoir: Nature, **385**, 426–428.

Dvorkin, J., and Nur, A., 1993, Rock physics for characterization of gas hydrates: The Future of Energy Gases, U.S. Geol. Survey Professional Paper 1570, pages 293–298.

Ecker, C., and Lumley, D. E., 1994a, Seismic AVO analysis of methane hydrate structures: 64th Ann. Internat. Meeting, Soc. Expl. Geophys., Expanded Abstracts, 1100–1103.

Ecker, C., and Lumley, D. E., 1994b, Seismic AVO analysis of methane hydrate structures: SEP–**80**, 277–292.

Ecker, C., Dvorkin, J., and Nur, A., 1996, Sediments with gas hydrates: Internal structure from seismic AVO: Geophysics, submitted for publication.

Ecker, C., 1995, Velocity structure of the methane hydrate formation at the Blake Outer Ridge: SEP–**84**, 109–124.

Ecker, C., 1997, Detecting S-wave velocity contrasts across BSRs using AVO: SEP–**94**, 17–31.

Hamilton, E. L., 1976, Shear-wave velocity versus depth in marine sediments: A review: Geophysics, **41**, 985–996.

Kvenvolden, K., 1993, Gas hydrates – geological perspective and global change: Reviews of Geophysics, **31**, 173–187.

Lee, M. W., Hutchinson, D. R., Dillon, W. P., Miller, J. J., Agena, W. F., and Swift, B. A., 1992, A method of estimating the amount of in situ gas hydrates in deep marine sediments: USGS Open File Report, **276**.

Lee, M. W., Hutchinson, D. R., Agena, W. F., Dillon, W. P., Miller, J. J., and Swift, B. A., 1994, Seismic character of gas hydrates on the southeastern U.S. continental margin: Marine Geophys. Res., **16**, 163–184.

Lumley, D. E., and Beydoun, W. B., 1993, Angle-dependent reflectivity estimation by Kirchhoff migration/inversion: Theory: SEP–**79**, 205–226.

Lumley, D. E., 1993, Kirchhoff prestack impedance inversion: A gas reservoir pilot study: SEP–**77**, 211–230.

Matsumoto, R., Paull, C., Wallace, P., and the Leg 164 Scientific party, 1996, Gas hydrate sampling on the Blake Ridge and Carolina Rise: ODP, Leg 164 Preliminary Report.

Warner, M., 1990, Absolute reflection coefficients from deep seismic reflections: Tectonophysics, **173**, 15–23.